Nuclear Instruments and Methods in Physics Research A 823 (2016) 126–134

Contents lists available at ScienceDirect

Nuclear Instruments and Methods in Physics Research A

journal homepage: www.elsevier.com/locate/nima

An investigation of medical radiation detection using CMOS image sensors in smartphones

Han Gyu Kang [a], Jae-Jun Song [b], Kwonhee Lee [c], Ki Chang Nam [d], Seong Jong Hong [e], Ho Chul Kim [e,*]

[a] Department of Senior Healthcare, Graduate School of Eulji University, Daejeon 301-746, Republic of Korea
[b] Department of Otorhinolaryngology-Head & Neck Surgery, Korea University, Guro Hospital,148, Gurodong-ro, Guro-gu, Seoul 152-703, Republic of Korea
[c] Graduate Program in Bio-medical Science, Korea University, 2511 Sejong-ro, Sejong City 339-770, Republic of Korea
[d] Department of Medical Engineering, College of Medicine, Dongguk University, 32 Dongguk-ro, Goyang-si, Gyeonggi-do 410-820, Republic of Korea
[e] Department of Radiological Science, Eulji University, 553 Yangji-dong, Sujeong-gu, Seongnam-si, Gyeonggi-do 431-713, Republic of Korea

ARTICLE INFO

Article history:
Received 5 February 2016
Received in revised form
2 April 2016
Accepted 3 April 2016
Available online 6 April 2016

Keywords:
Radiation detection
X-ray
Gamma-ray
Smartphone
CMOS

ABSTRACT

Medical radiation exposure to patients has increased with the development of diagnostic X-ray devices and multi-channel computed tomography (CT). Despite the fact that the low-dose CT technique can significantly reduce medical radiation exposure to patients, the increasing number of CT examinations has increased the total medical radiation exposure to patients. Therefore, medical radiation exposure to patients should be monitored to prevent cancers caused by diagnostic radiation. However, without using thermoluminescence or glass dosimeters, it is hardly measure doses received by patients during medical examinations accurately. Hence, it is necessary to develop radiation monitoring devices and algorithms that are reasonably priced and have superior radiation detection efficiencies. The aim of this study is to investigate the feasibility of medical dose measurement using complementary metal oxide semiconductor (CMOS) sensors in smartphone cameras with an algorithm to extract the X-ray interacted pixels. We characterized the responses of the CMOS sensors in a smartphone with respect to the X-rays generated by a general diagnostic X-ray system. The characteristics of the CMOS sensors in a smartphone camera, such as dose response linearity, dose rate dependence, energy dependence, angular dependence, and minimum detectable activity were evaluated. The high energy gamma-ray of 662 keV from Cs-137 can be detected using the smartphone camera. The smartphone cameras which employ the developed algorithm can detect medical radiations.

1. Introduction

The use of radiation in medicine has increased annually with the improvements of medical imaging devices such as general radiographic X-ray equipment, X-ray fluoroscopy, computed tomography (CT), single photon emission computed tomography (SPECT), and positron emission tomography (PET). As a result, the radiation exposure doses for patients and medical staff have also increased, which could potentially be hazardous for the health of both patients and staff. For these reasons, the medical radiation exposures to patients and staff should be monitored and managed carefully to prevent the potential health hazards. On top of that, the awareness of radiation danger has also increased dramatically since the nuclear accidents at Fukushima, Japan in March 2011.

Consequently, the concerns of medical radiation exposure and nuclear reactor accidents have increased the demand of a personnel dosimeter which can be used easily at a reasonable price.

The Geiger–Müller (G–M) counter has been used widely as a survey metre to measure radiation exposure dose in hospital and industrial field. However, it is not affordable to be used as a personal dosimeter, because the GM counter is bulky and expensive. Besides the limited number of GM counters makes it difficult for public to use the GM counter as a personal dosimeter.

The scintillation detector which uses a combination of a scintillator and semi-conductor detector, can provide an excellent detection efficiency for high energy gamma rays with energy information. Despite the fact that the scintillation detector can be manufactured in a small size while maintaining the excellent performances, it is unaffordable to public due to the expensive price.

On the other hand, the complementary metal-oxide semiconductor (CMOS) image sensors of smartphone cameras can detect not only visible light but also ionizing radiations such as ultraviolet ray, X-ray, and high energy gamma-ray [1–3]. The

* Corresponding author.

http://dx.doi.org/10.1016/j.nima.2016.04.007
0168-9002/

potential of smartphone camera as a gamma-ray detector has been demonstrated and the application software called GammaPix was developed [4]. Also the usability of smartphones for dose alerts was investigated with an android application software called Radioactive Counters [5,6].

The smartphones have become ubiquitous rapidly throughout the world. The performances of smartphone camera, such as camera pixel depth, camera frame rate and computing speed also have been accelerated, which makes it easier to extract and analyze X-ray informations obtained by smartphone cameras.

In order to use smartphones as a radiation warner, the radiation responses of the smartphones should be characterized carefully [7]. We developed an algorithm to extract and characterize radiation induced pixel intensity from the thermal noise of the CMOS sensors in smartphones. The aim of this study is to investigate the feasibility of smartphone CMOS image sensors as a radiation warner for medical radiation, such as X-rays and gamma rays.

2. Experimental set-up

2.1. X-ray detection using CMOS image sensors in smartphone

The smartphone camera was wrapped with black tape to allow the CMOS image sensor of the front camera to interact with X-rays and gamma-rays while blocking visible light rays. The Galaxy S2 smartphone (Samsung Electronics, SHW-M250S, South Korea) was operated in a video recording mode while the smartphone camera was irradiated by X-rays switched on 10 s after the video recording has started using a diagnostic general radiographic X-ray system (Choongwae Medical, CXD-RI55, South Korea) as shown in Fig. 1. The anode angle of the tungsten target was 17°. The intrinsic filtration was 2 mm thick aluminium and additional filtration was 1.0 mm thick aluminium.

The distance between the focus of the X-ray tube to the surface of the smartphone camera was 100 cm. The field size of the X-ray beam was $10 \times 10\ cm^2$ which can cover the entire ion chamber length of 10 cm as shown in Fig. 1(c). The ion chamber which has a volume of 3.14 cc and an effective length of 10 cm (Type 30,009, PTW, UNIDOS®, Germany), was positioned alongside the smartphone to measure accurate doses and dose rates. The measured doses and dose rates of the ion chamber were used to evaluate the X-ray responses of the smartphone CMOS image sensor such as dose linearity, dose rate and X-ray energy dependence as well as angular dependence.

3. Image processing for extraction of radiation detected pixels on smartphone

The front camera in the display screen side has a matrix size of 640×480 (307,200 pixels), and the rear camera has a matrix size of 1920×1080 (2073,600 pixels) with a bit depth of 8. The video was recorded at a frame rate of 25 fps in MPEG-4 format during the X-ray irradiation. The video file was imported by MATLAB R2012a (MathWorks Inc., USA), then split into individual frames. The frames from the 0–3 s were discarded, because they usually contain some sparkle noises.

The total pixel intensity of the frame I can be calculated by the following Eq. (1).

$$I = \sum_{x=1}^{m} \sum_{y=1}^{n} f(x, y) \tag{1}$$

Where, $f(x, y)$ represents the pixel intensity of the frame at the x-and y-coordinates, m and n represent total number of rows and columns of the frame respectively.

The noise level was calculated by using Eqs. (2) and (3).

$$\text{Noise level} = \bar{I}_N + 3\sigma_N \tag{2}$$

where, $\bar{I}_N$ and σ_N represent the average and standard deviation of the total pixel intensity of the frames between the interval 3–5 s which corresponds to the frame number of 75–125.

$$\bar{I}_N = \frac{1}{50} \sum_{k=75}^{125} I_k, \quad \sigma_N = \sqrt{\frac{1}{50} \sum_{k=75}^{125} (I_k - \bar{I}_N)^2} \tag{3}$$

The value k is the frame number and I_k is the total pixel intensity of the frame at the frame number k.

The frame exceeding the noise levels of the each red, green and blue component was extracted as a radiation-interacted frame. Subsequently, the frame was converted to the grey scale and the total pixel intensity of the frame was calculated. In order to reject the noise pixel intensity from the radiation interacted frame, the average noise value $\bar{I}_n$ was subtracted from the total pixel intensity of the radiation interacted frame by the following Eq. (4).

$$\text{Radiation induced pixel intensity} = I_R - \bar{I}_N \tag{4}$$

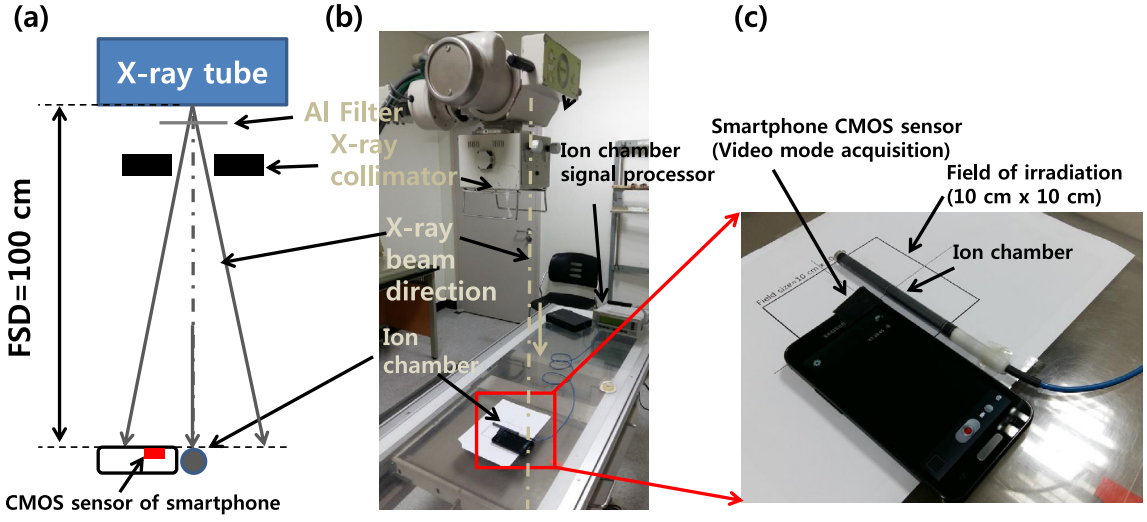

Fig. 1. Schematic diagram and photographs of the experimental setup for radiation detection with the smartphone: (a) schematic and (b) experimental setup for radiation detection with the smartphone, and (c) ion chamber with the smartphone inside the $10\ cm^2$ X-ray irradiation field.

Where, I_R represents the total pixel intensity of the radiation-interacted frame before the noise subtraction, and $\bar{I}_N$ represents the average total pixel intensity of the frames between the interval 3–5 s.

The pixels which have the intensities of less than 5 were mostly induced by the thermal noise of the CMOS image sensors [8]. Therefore, the radiation-interacted number of pixels per frame was calculated by counting the pixels which exceed the pixel intensity value of 4.

The cumulative radiation induced pixel intensity which hereafter will be referred to as a pixel intensity, was calculated by adding all of the radiation induced pixel intensities of the frames interacted with the radiation.

4. X-ray responses of the smartphone camera

4.1. X-ray detection using the smartphone CMOS image sensors

Fig. 2(a) shows the smartphone camera image without X-ray exposure. Fig. 2(b) and (c) shows the smartphone camera images for the tube current of 50 mA and 100 mA respectively. The tube voltage of 80 kV and exposure time of 1 s were used. The R, G, and B pixel intensities as a function of frame number were plotted as shown in the top row of the Fig. 2.

Fig. 3(a) and (b) shows the pixel intensities and the number of pixels as a function of ion chamber dose for the red, blue, green, and grey components. The tube current was varied from 20 mA to 250 mA, while the tube voltage, exposure time, and focus-to-surface distance (FSD) were fixed to 80 kV, 50 ms, and 100 cm respectively. An excellent linear relationship was obtained between the pixel intensities and the ion chamber dose, and the blue component showed higher sensitivity compared to the red and green components as shown in Fig. 3(a). However the number of radiation-interacted pixel was not increased linearly as a function of the ion chamber dose as shown in Fig. 3(b).

4.2. Dose linearity (X-ray)

The dose linearity of the front camera was evaluated with different doses. The tube voltage, exposure time and FSD were set to 80 kV, 50 ms, and 100 cm respectively as described in the Section 4.1. We increased the tube current from 20 mA to 250 mA to deliver different doses to the smartphone camera and the ion chamber. The measurements of dose using the smartphone camera and the ion chamber were repeated three times to check the reproducibility. The pixel intensity in grey scale were plotted as a function of the ion chamber dose as shown in Fig. 4(c). The pixel intensity of the front camera and the dose value of the ion chamber were increased linearly as the tube current was increased as shown in Fig. 4(a) and (b). Fig. 4(c) shows an excellent linear relationship between the pixel intensity and the ion chamber dose.

However, the maximum and average coefficient of variation were 10.4% and 4.9% respectively, which are relatively larger than those of the ion chamber as shown in Table 1.

4.3. Dose rate dependence (X-ray)

The X-ray dose rate dependence was investigated by varying the FSD from 110 cm to 35 cm with a 5 cm step. The tube voltage and exposure time were fixed to 80 kV and 50 ms respectively. The X-ray irradiation field was also fixed to 10 cm × 10 cm regardless of the FSD variation to deliver the same amount of dose to both the smartphone camera and ion chamber. The tube currents of 100 mA and 200 mA were used to investigate the dose rate dependence.

In case of the tube current of 100 mA, the pixel intensity and the absorbed dose of the ion chamber were inverse-squarely varied to the FSD as shown in Fig. 5(a). The pixel intensity was increased linearly as a function of dose rate as shown in Fig. 5(b). A linear regression line was fitted excluding the last data point of 730 mGy/h to check the linearity of pixel intensity with respect to the dose rate as shown in Fig. 5(b). The pixel intensity was not saturated up to the dose rate of 544 mGy/h as shown in Fig. 5 (a) and (b).

However, the pixel intensity was saturated from the dose rate

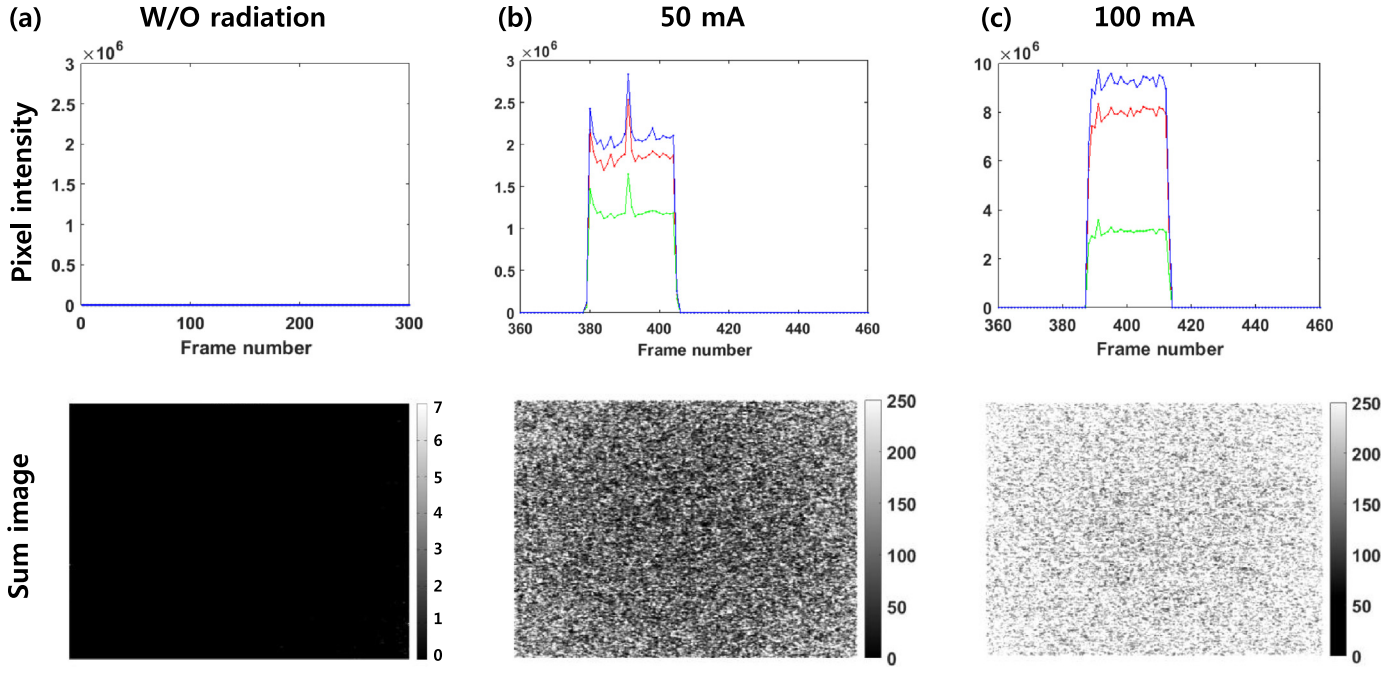

Fig. 2. Smartphone images with different tube currents: (a) pixel intensity as a function of frame number and sum image without X-ray irradiation, (b) tube current of 50 mA, and (c) tube current of 100 mAs. (Tube voltage and exposure time were constant to 80 kV and 1 s respectively).

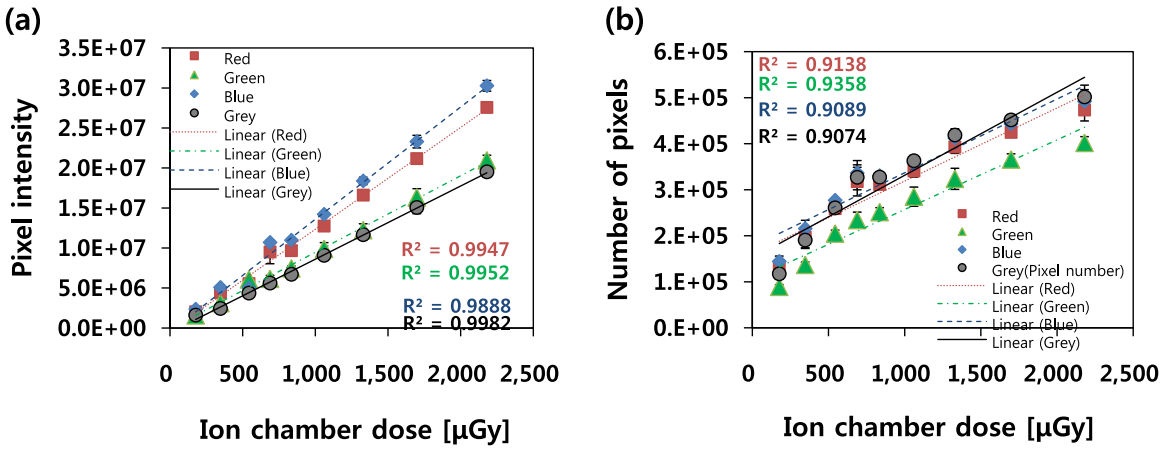

Fig. 3. Comparison of dose linearity between pixel intensity and pixel number: (a) pixel intensities as a function of dose, and (b) the number of pixels as a function of dose.

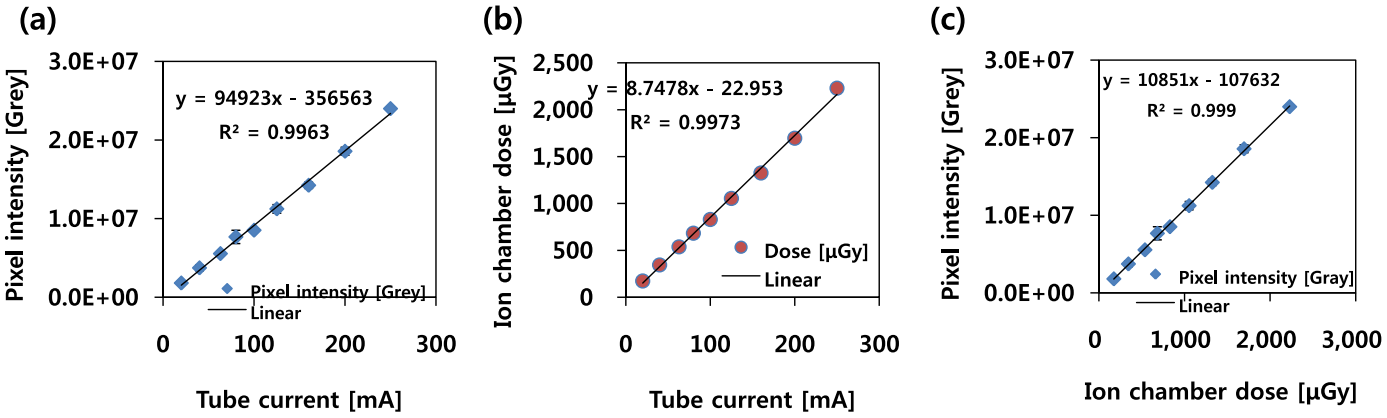

Fig. 4. Pixel intensity and ion chamber dose with different tube currents: (a) pixel intensity as a function of tube current, (b) ion chamber dose as a function of tube current, and (c) pixel intensity as a function of ion chamber dose.

Table 1
Pixel intensity and ion chamber dose with different tube currents.

	Ion chamber dose			Smartphone (Front camera)		
Tube current [mA]	Mean [μGy]	SD [μGy]	CV [%]	Mean [Pixel intensity]	SD [Pixel intensity]	CV [%]
20	174	2.0	0.1	1.61×10^6	1.29×10^5	8.0
40	344	1.5	0.4	2.44×10^6	2.54×10^5	10.4
63	538	1.5	0.3	4.36×10^6	2.12×10^5	4.9
80	683	1.0	0.1	5.62×10^6	1.78×10^5	3.2
100	830	1.5	0.2	6.72×10^6	2.64×10^5	3.9
125	1054	2.0	0.2	9.08×10^6	1.07×10^5	1.2
160	1325	3.0	0.3	11.67×10^6	4.65×10^5	4.0
200	1696	2.1	0.1	15.07×10^6	7.85×10^5	5.2
250	2229	11.0	0.5	19.528×10^6	6.63×10^5	3.4

Note, SD:Standard deviation, CV:Coefficient of variation. Each measurement was repeated three times. (Tube voltage=80 kV, exposure time=50 ms, focus-to-surface distance=100 cm).

of 845 mGy/h with the tube current of 200 mA as shown in Fig. 6(b). As a result the pixel intensity was not inversely proportional to the FSD as shown in Fig. 6(a).

4.4. X-ray energy dependence

The X-ray energy dependence of the smartphone's front camera was investigated with different tube voltages. The energy spectra and mean photon energy with different tube voltages were obtained by SRS-78 simulation software as shown in Fig. 7(a) and (b) [9]. The simulated mean photon energies were 28.4 keV, 36.4 keV, 43.5 keV, 49.8 keV, 55.0 keV, and 59.7 keV for 40 kV, 60 kV, 80 kV, 100 kV, 120 kV, and 140 kV respectively.

The simulated absorbed doses obtained by SRS-78 simulation, showed a good agreement with the measured absorbed dose by the ion chamber as shown in Fig. 7(b). The pixel intensity and ion chamber dose increased with tube voltage according to a power law (proportional to kV2.4) as shown in Fig. 8(a) and (b).

The pixel intensity was linearly increased regardless of the mean photon energy of the X-rays ranging from 28.4 to 59.7 keV as shown in Fig. 8(c).

4.5. Angular dependence on X-ray

The pixel intensity and pixel number of the front camera were dependent on the incoming of the X-rays as shown in Fig. 9(b) and Table 2. When the X-rays were irradiated on the normal incident angle (0°) to the smartphone's front camera, the pixel intensity and pixel number showed the maximum values compared to the other incident angles. However as the smartphone was rotated the pixel intensity was decreased. The relative pixel intensity and pixel number of the front camera were 6% and 11% as the X-rays were irradiated with incoming angle of −90°. The average absorbed dose measured by the ion chamber was 471 ± 7 μGy. The FSD, tube voltage, tube current, and exposure time were set to constant to 100 cm, 80 kV, 100 mA, and 50 ms respectively.

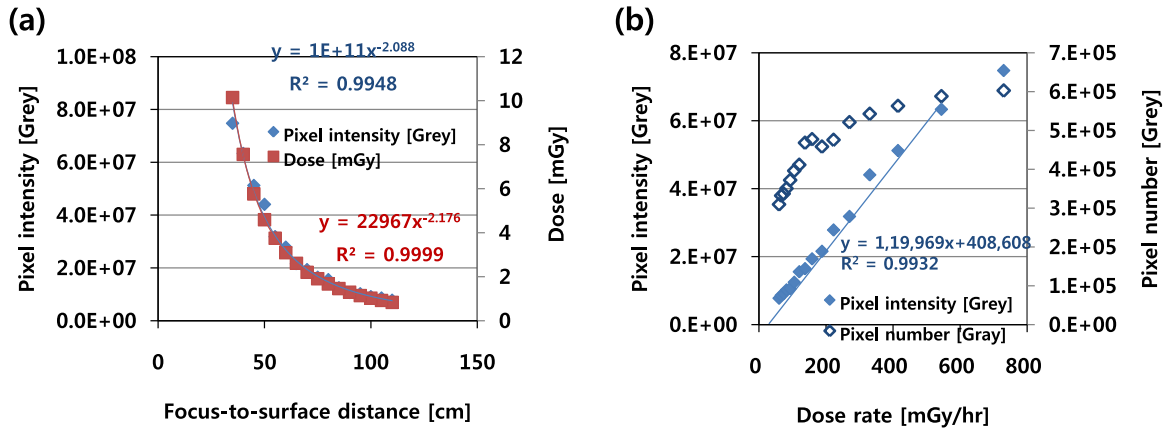

Fig. 5. (a) Pixel intensity and ion chamber dose as a function of the FSD, (b) pixel intensity and pixel number as a function of dose rate. (Tube current=100 mA).

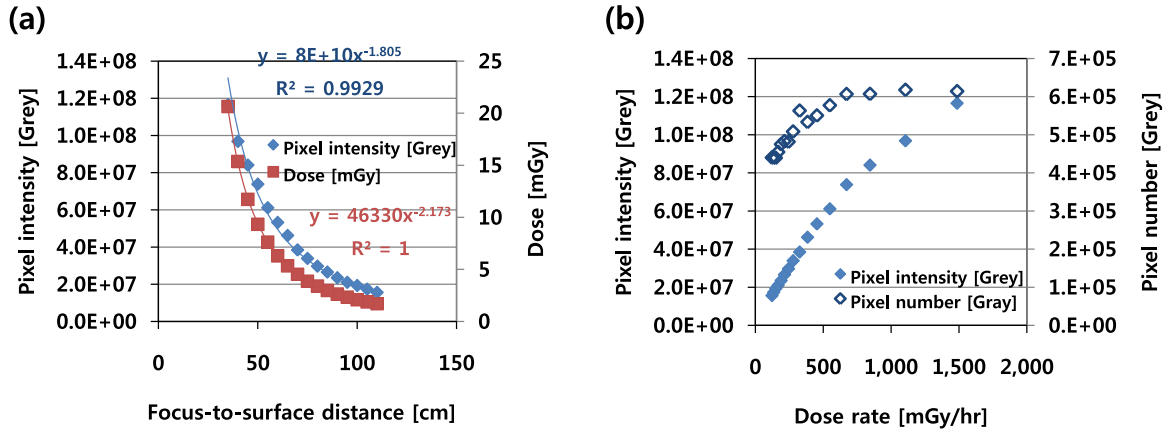

Fig. 6. (a) Pixel intensity and ion chamber dose as a function of the FSD, (b) pixel intensity and pixel number as a function of dose rate. (Tube current=200 mA).

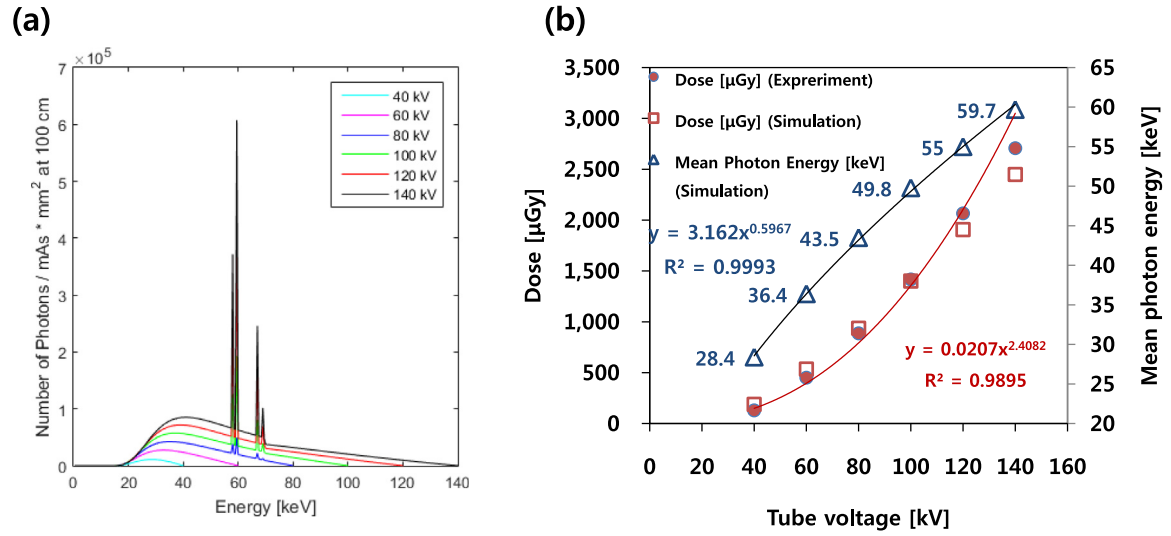

Fig. 7. (a)SRS-78 energy spectrum simulation results with different tube voltages, (b) measured and simulated absorbed doses and mean photon energy (simulation) as a function of tube voltage.

5. Gamma-ray response of the smartphone camera

Fig. 10 shows the responses of the front camera without and with Cs-137. Without the Cs-137 irradiation, both of the average pixel intensity and the number of pixels per frame were less than 1 during the 3 min acquisition time as shown in Fig. 10(b) and (c). When the front camera of the smartphone was irradiated with Cs-137 with a dose rate of 60 μSv/h for 3 min, the pixel intensity and the number of pixels were increased significantly compared to without the Cs-137 irradiation as shown in Fig. 10(e) and (f). With the Cs-137 irradiation, the frame number 1775 was found to have the maximum grey value and its image can be seen in Fig. 10(d).

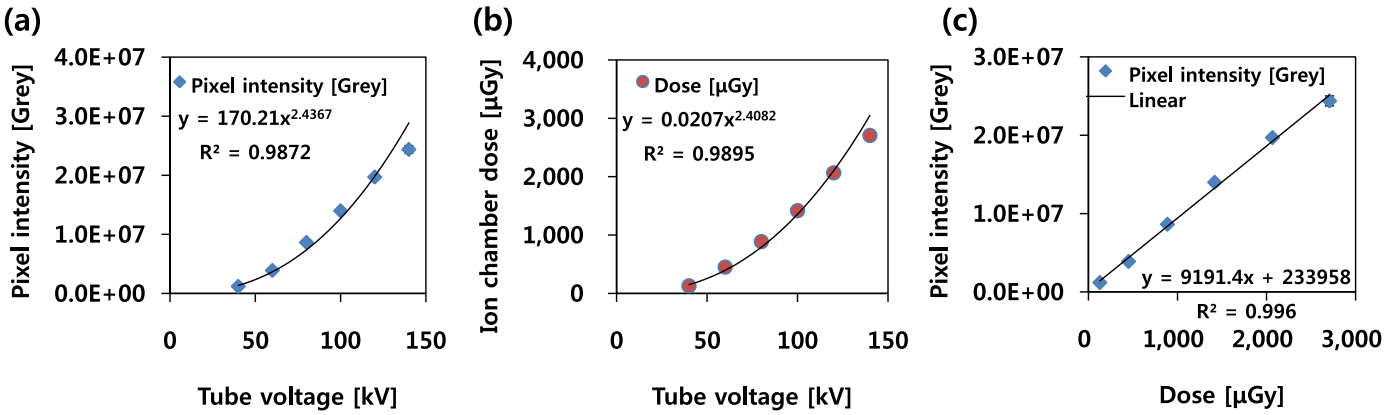

Fig. 8. (a) Pixel intensity as a function of tube voltage. (b) Ion chamber dose as a function of tube voltage, and (c) pixel intensity as a function of dose.

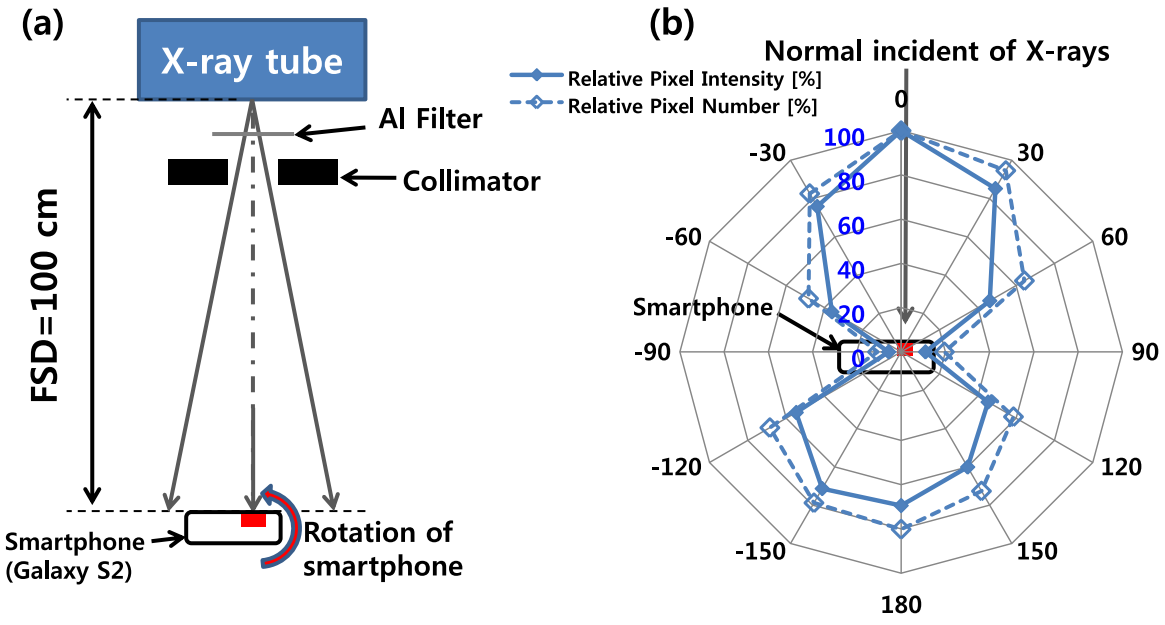

Fig. 9. (a) Experimental setup for angular dependence test with smartphone camera, (b) angular dependence of the smartphone's front camera on X-ray.

Table 2
Pixel intensity and pixel number with different incoming X-ray angles.

	Smartphone (Front camera)							
X-rays incoming angle [°]	Relative pixel intensity [%]	Mean [Pixel intensity]	SD [Pixel intensity]	CV [%]	Relative pixel number [%]	Mean [Pixel number]	SD [Pixel number]	CV [%]
0	100	9.49×10^6	7.80×10^5	8.2	100	3.54×10^5	2.20×10^4	6.2
30	85	8.09×10^6	2.59×10^5	3.2	95	3.35×10^5	1.64×10^4	4.9
60	46	4.39×10^6	3.19×10^5	7.3	64	2.28×10^5	2.97×10^4	13.0
90	*11*	1.04×10^6	1.11×10^5	10.7	20	0.63×10^4	0.79×10^4	11.4
120	*45*	4.31×10^6	3.61×10^5	8.4	59	2.07×10^5	1.48×10^4	7.1
150	*60*	5.70×10^6	4.00×10^5	7.0	73	2.57×10^5	1.81×10^4	7.0
180	*69*	6.59×10^6	2.46×10^5	3.7	80	2.84×10^5	2.01×10^4	7.1
−150	*71*	6.77×10^6	5.98×10^5	8.8	79	2.79×10^5	2.59×10^4	9.3
−120	*55*	5.20×10^6	3.39×10^5	6.5	68	2.42×10^5	1.26×10^4	5.2
−90	*6*	0.54×10^6	0.57×10^5	10.6	11	0.38×10^5	0.37×10^4	9.9
−60	*36*	3.43×10^6	3.47×10^5	10.1	48	1.71×10^5	1.72×10^4	10.0
−30	*76*	7.20×10^6	1.93×10^5	2.7	83	2.92×10^5	0.87×10^4	3.0

Note, SD:Standard deviation, CV:Coefficient of variation. Each measurement was repeated three times. (Tube voltage=80 kV).

The four spots of the frame number 1775 were created by the gamma-ray interaction with the front camera as shown in Fig. 10 (d). The number of pixels in Fig. 10 (c) and (f) were converted into counts per minute (cpm) value by averaging the number of pixels over Cs-137 irradiation time of 3 min. In case of without Cs-138 irradiation, the counts per minute value were 0, 0, 0, and 0 for red,

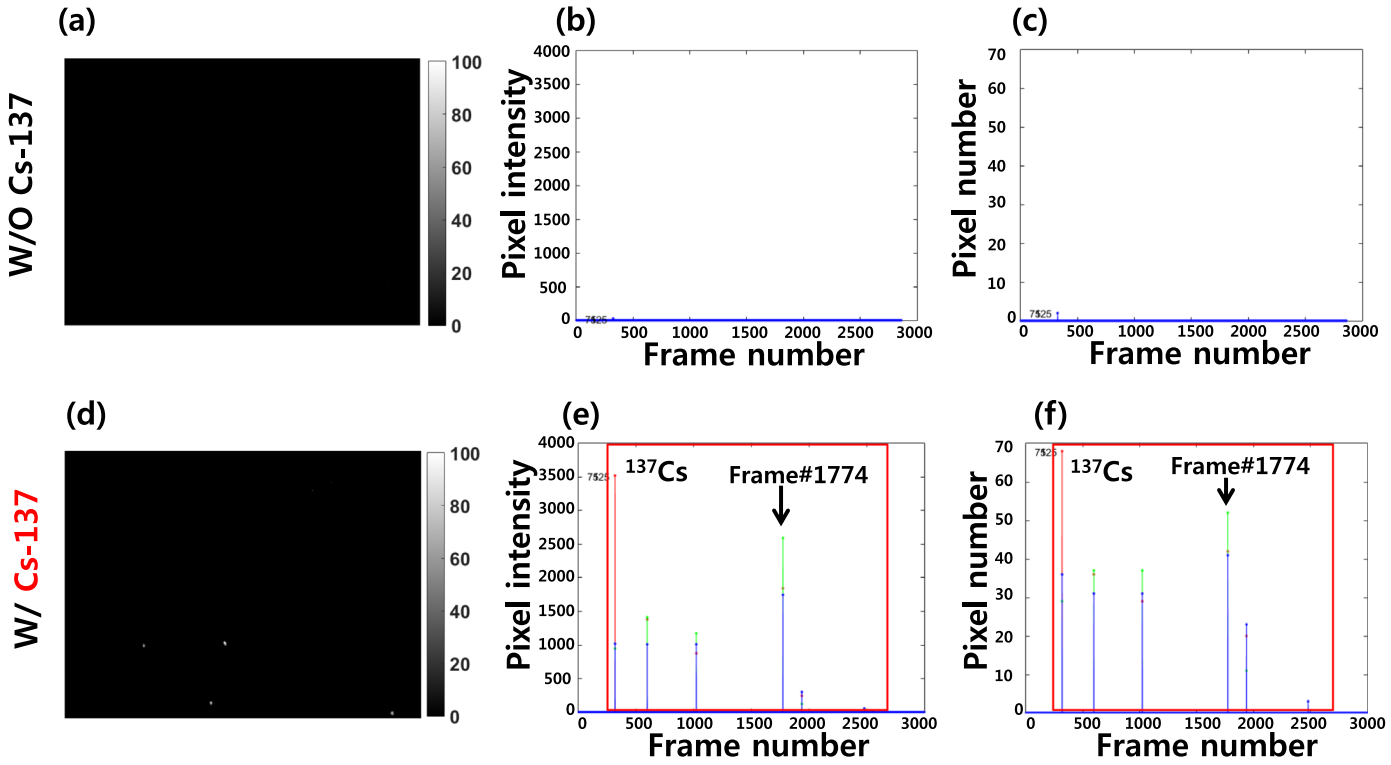

Fig. 10. Smartphone responses with and without the Cs-137 irradiation: (a) image of the frame number 75 without Cs-137, (b) pixel intensity as a function of time without Cs-137, (c) number of pixels as a function of time without Cs-137, (d) image of the frame number 1774 with Cs-137 irradiation, (e) pixel intensity as a function of time with Cs-137, and (f) number of pixels as a function of time with Cs-137.

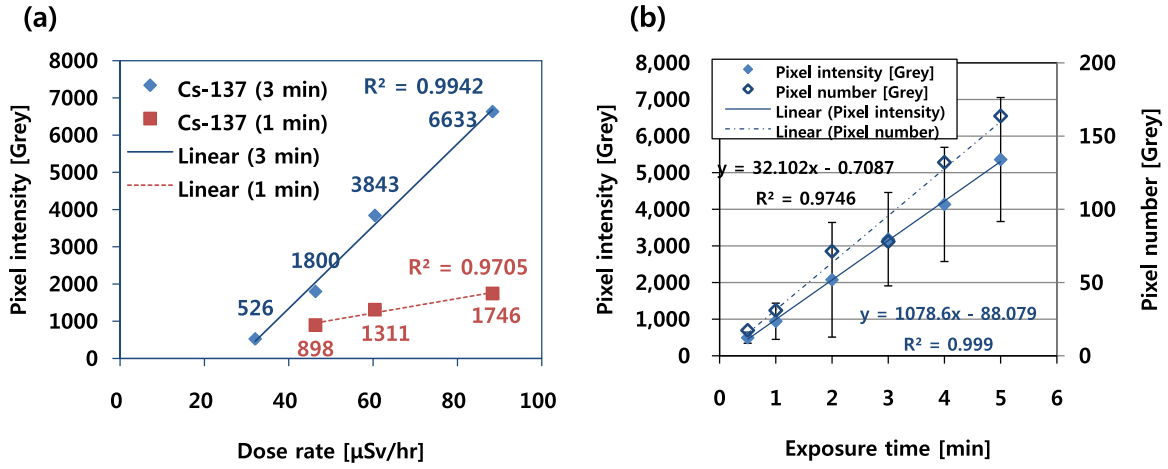

Fig. 11. (a) Pixel intensity as a function of dose rate of Cs-137, (b) pixel intensity and pixel number as a function of Cs-137 (62 μSv/h) exposure time (The error bars indicate the standard deviation of the pixel intensity with three times measurements).

blue, green, and grey components respectively. In case of with Cs-137 irradiation for 3 min, the counts per minute value were 71, 61, 60, and 74 for red, blue, green, and grey components respectively.

5.1. Gamma-ray dose rate dependence

The dose rate dependence of the front camera was evaluated by varying the distance between the radioactive nuclide source to the front camera. The dose rate (μSv/h) as a function of the source-to-detector distance (SDD) were measured by a survey metre (ASM-990, Fluke, USA) coupled with a pancake probe (Model 489-110D, Fluke, USA). The different dose rates were irradiated by changing the SDD with an 1 cm step. The gamma rays emitted from the nuclides were irradiated for 3 min to the smartphone's front camera to reduce the statistical variation on the measured pixel intensity.

The pixel intensity of the front camera increased linearly as the dose rate of the Cs-137 (662 keV) increased as shown in Fig. 11(a). With the exposure time of 3 min, the front camera was not able to detect the 662 keV gamma-rays as the dose rate was lower than 32 μSv/h. The pixel intensity and the number of pixels were increased linearly as a function of the Cs-137 exposure time with the dose rate of 62 μSv/h as shown in Fig. 11(b).

5.2. Gamma-ray energy dependence (^{133}Ba, ^{137}Cs, ^{60}Co)

In order to investigate the gamma-ray energy dependence of the front camera, various nuclides such as Ba-133, Cs-137 and Co-

Table 3
Summary of the radionuclides properties [10].

Nuclide	Energy [keV]	HVL [mm]	Γ-constant [mSv/h/MBq]	Half-life [days]
Ba-133	81 (31%) 356 (62%)	1	7.80×10^5	271
Cs-137	662 (85%)	10	2.59×10^5	11,012
Co-60	1173 (99%) 1333 (99%)	16	3.19×10^5	1924

60 were used and their properties are summarized as shown in Table 3 [10].

The pixel intensities obtained for 3 min of gamma-rays irradiation were increased linearly by the dose rate with different nuclides such Ba-133, Cs-137, and Co-60 as shown in Fig. 12(a). The counts per minute was obtained by averaging the pixel numbers over 3 min as shown in Fig. 12(b). The pixel intensity and counts per minute showed linear relationship with dose rate of different nuclides. In case of the dose rate of 80 μSv/h, the relative pixel number of the front camera were 100%, 44%, and 19% for Ba-133, Cs-137, and Co-60 respectively as shown in Fig. 12(b).

5.3. Minimum detectable dose rate (^{133}Ba, ^{137}Cs, ^{60}Co)

In case of the exposure time of 3 min, the minimum detectable dose rates of the Ba-133, Cs-137 and Co-60 were 3.9 μSv/h, 32.0 μSv/h, and 30.2 μSv/h respectively. As the exposure time was decreased from 3 min to 1 min, the minimum detectable dose rates were increased to 4.8 μSv/h, 46.3 μSv/h, and 37.8 μSv/h respectively.

6. Discussion

The smartphone CMOS image sensor and proposed algorithm can detect either X-rays or gamma-rays. The radiation interacted frame, pixel intensity and the number of pixels can be obtained by subtracting the noise level of the camera as shown in Fig. 2.

The pixel intensity of the Samsung Galaxy S2 front camera increased linearly as the X-ray dose increased. The average coefficient of variation of the pixel intensity was 4.9% which is about 10 times higher than that of the 0.4% of the ion chamber. This is mainly because the detection efficiency of the CMOS image sensor is lower than the ion chamber with respect to the X-rays.

In case of the X-ray irradiation with a tube voltage of 80 kV, the pixel number and pixel intensity were saturated from the dose rate of 380 mGy/h and 845 mGy/h respectively as shown Fig. 5(b). Therefore, a large dimension of pixel matrix with a high pixel depth will be preferable for the detection of high dose rate of radiations.

As the X-rays were irradiated into the CMOS image sensor of the front camera of the Galaxy S2 smartphone with an incoming angle of 0°, the pixel intensity and pixel number were 9490,126 ± 780,137 and 354,011 ± 22,014 respectively as described in the Section 4.5. These results indicate that the at least more than one pixel element was activated on the CMOS image sensor of the smartphone, as a result of the X-ray interaction with the CMOS image sensor. The sigma values of the pixel intensity and the pixel number represent the standard deviations of repeated measurements with 3 times.

Since the pixel intensity and pixel number of the smartphone camera were strongly dependent on the incoming angle of the X-rays as shown in Fig. 9(b), the smartphone should be aligned in the right direction when detecting radiation. The angular dependence of the smartphone camera with respect to incoming X-ray or gamma ray, makes it hard to be used as a reliable radiation dosimeter [5,6]. Therefore, the possible use of smartphone camera is just warning the presence of radioactive materials in radiological incident environment.

A glass focusing lens with a thickness of 2 mm is placed on the surface of smartphone camera. In general the density of glass is 2.5 g/cm^2, while the mass attenuation coefficient of the glass 0.4341 cm for photon energy of 40 keV [11]. Hence, the half value layer of the glass for photon energy of 40 keV is 0.64 cm [12]. The glass lens with a 2 mm thickness on the surface of the CMOS image sensor blocks about 14% of incoming X-rays of 40 keV. The fractions of absorbed or scattered x-ray by the glass lens are 11%, 9%, 8%, and 7% for X-ray energies of 50 keV, 60 keV, 80 keV, and 100 keV respectively. In case of the gamma ray energy of 662 keV (Cs-137), the fraction of attenuated gamma photons is only 3%. Therefore, the detection efficiency of low energy X-ray can be affected by the glass lens on the surface of CMOS image sensor. The radionuclides such as Ba-133, Cs-137 and Co-60, can be detected by using the smartphone camera. The pixel intensity increased linearly as the dose rate of the radionuclides increased as shown in Fig. 11(a). The pixel intensity and pixel number were also increased linearly with the radionuclides exposure time as shown Fig. 11(b).

The pixel number decreased as the gamma-ray photon energy increased as shown in Fig. 12(c). This is because the CMOS image sensor has a thickness of less than 10 μm. Thus, the energy dependence of the smartphone camera should be taken to account for an accurate measurement of dose and dose rate.

The minimum detectable dose rates of the front camera were 3.9 μSv/h, 32.0 μSv/h, and 30.2 μSv/h for Ba-133, Cs-137, and Co-

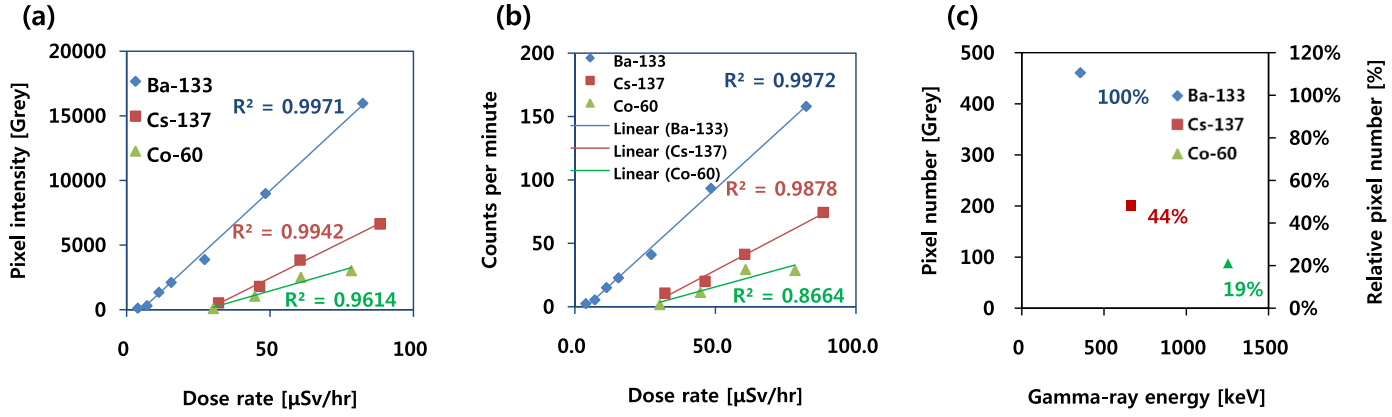

Fig. 12. (a) Pixel intensities as a function of dose rate with different nuclides, (b) counts per minute as a function of dose rate with different nuclides, and (c) relative pixel intensity with different gamma-ray energies.

60 respectively as the radionuclides were irradiated for 3 min. The minimum detectable dose rates increased as the exposure time decreased from 3 min to 1 min. The tradeoff between the minimum detectable dose rate and exposure time will be optimized by improving the algorithm for the extraction of radiation interacted pixel in the further study.

In this study, all of the video files recorded by the smartphones were processed using Matlab software rather in real time. Thus, real time dose measurement using the smartphones could not be performed in this study. In the future study, the proposed extraction algorithm of the radiation detected pixel signal will be implemented to a smartphone for real time dose monitoring.

7. Conclusion

We demonstrated the feasibility of radiation detection using smartphone cameras. The extraction algorithm of the radiation interacted pixels from the video file was developed successfully. The smartphone camera can be used to detect either X-ray and high energy gamma-ray such as 662 keV photon emitted from Cs-137. Since the smartphones showed a significant angular dependence on X-ray and energy dependence on gamma ray, the smartphones cannot be used as a reliable dosimeter but a dose warner.

Acknowledgement

This work was supported by grants from the Korean Research Foundation funded by the Korean Government (NRF-2015M2B2A9033015).

References

[1] D. Igoe, A. Parisi, B. Carter, Characterization of a smartphone camera's response to ultraviolet A radiation, Photochem. Photobiol. 89 (2013) 215–218.
[2] J.J. Cogliati, K.W. Derr, J. Wharton, Using CMOS Sensors in a Cellphone for Gamma Detection and Classification, arXiv:1401.0766 (physics.ins-det), 2014.
[3] F. WANG, M.-Y. WANG, Y.-F. LIU, C.-W. MA, L. CHANG, Obtaining low energy γ dose with CMOS sensors, Nucl. Sci. Techn. 25 (2014) 060401.
[4] G.A. Drukier, E.P. Rubenstein, P.R. Solomon, M.A. Wojtowicz, M.A. Serio, Low cost, pervasive detection of radiation threats, technologies for homeland security (HST), in: Proceedings of the 2011 IEEE International Conference, 2011, pp. 365–371.
[5] T. Kaireit, G. Stamm, C. Hoeschen, F.K. Wacker, Usability of smartphones for dose alerts, RoFo 185 (2013) 558–562.
[6] H. Hartmann, V. Hietschold, R. Freudenberg, J. Kotzerke, Dresden, smartphones now even smarter – Possibility of using a "dose warner", RoFo 185 (2013) 1207.
[7] O. Van Hoey, A. Salavrakos, A. Marques, A. Nagao, R. Willems, F. Vanhavere, V. Cauwels, L.F. Nascimento, Radiation dosimetry properties of smartphone CMOS sensors, Radiat. Prot. Dosim. 168 (2016) 314–321.
[8] H. Tian, B. Fowler, E. Gamal, Analysis of temporal noise in CMOS photodiode active pixel sensor, IEEE J. Solid-State Circuits 36 (2001) 10.
[9] R. Birch, M. Marshall, Computation of Bremsstrahlung X-ray spectra and comparison with spectra measured with a Ge(Li) detector, Phys. Med. Biol. 24 (1979) 505.
[10] D.S. Smith, M.G. Stabin, Exposure rate constants and lead shielding values for over 1100 radionuclides, Health Phys. 102 (2012) 271–291.
[11] J.H. Hubbell, S.M. Seltzer, Tables of X-ray mass attenuation coefficients and mass energy-absorption coefficients 1 keV to 20 MeV for elements $z=1$–92 and 48 additional substances of dosimetric interest, Other Information: PBD: May 1995, pp. Medium: P; Size: 116p.
[12] J.H. Hubbell, Review of photon interaction cross section data in the medical and biological context, Phys. Med. Biol. 44 (1999) 22.